ACS OMEGA

http://pubs.acs.org/journal/acsodf

Article

Evaluation of CO_2 Absorption by Amino Acid Salt Aqueous Solution Using Hybrid Soft Computing Methods

Amir Dashti,* Farid Amirkhani, Amir-Sina Hamedi, and Amir H. Mohammadi*

Cite This: *ACS Omega* 2021, 6, 12459−12469

Read Online

ACCESS | Metrics & More | Article Recommendations

ABSTRACT: Amino acid salt (AAs) aqueous solutions have recently exhibited a great potential in CO_2 absorption from various gas mixtures. In this work, four hybrid machine learning methods were developed to evaluate 626 CO_2 and AAs equilibrium data for different aqueous solutions of AAs (potassium sarcosinate, potassium L-asparaginate, potassium L-glutaminate, sodium L-phenylalanine, sodium glycinate, and potassium lysinate) gathered from reliable references. The models are the hybrids of the least squares support vector machine and coupled simulated annealing optimization algorithm, radial basis function neural network (RBF-NN), particle swarm optimization−adaptive neuro-fuzzy inference system, and hybrid adaptive neuro-fuzzy inference system. The inputs of the models are the CO_2 partial pressure, temperature, mass concentration in the aqueous solution, molecular weight of AAs, hydrogen bond donor count, hydrogen bond acceptor count, rotatable bond count, heavy atom count, and complexity, and the CO_2 loading capacity of AAs aqueous solution is considered as the output of the models. The accuracies of the models' results were verified through graphical and statistical analyses. RBF-NN performance is promising and surpassed that of other models in estimating the CO_2 loading capacities of AAs aqueous solutions.

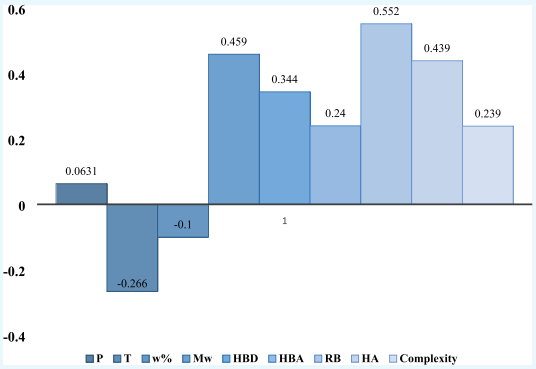

1. INTRODUCTION

Carbon dioxide (CO_2) footprint is one of the most impactful environmental issues contributing to global warming. Various human activities such as deforestation, fossil fuel combustion for transportation, industries, and so on are the main sources of CO_2 emission.[1,2] Climate change due to greenhouse gases is now threatening our habitation on earth more than ever; therefore, scientists are actively upgrading CO_2 capture technologies to mitigate CO_2 pollution. These technologies can be generally categorized into pre-combustion, oxy-combustion, and post-combustion levels.[3,4] Adsorption, cryogenic separation, membrane separation, absorption, and so on are examples for the abovementioned classification.[5−9] The most prevalent technique among them is chemical absorption due to its high absorption rate and capacity.[10] However, a suitable solvent selection comprises multiple facets such as CO_2 loading capacity, absorption/desorption rate, regeneration rate, toxicity, corrosion, volatility, and so on.[11]

Alkanolamine aqueous solutions and other types of amine aqueous solutions of primary, secondary, tertiary, and sterically hindered amine solutions have been used and proposed for CO_2 capturing from flue and industrial gas streams. One of the most widely used chemical absorbents among them is the aqueous monoethanolamine (MEA) solution featuring a fast absorption rate, acceptable thermal stability, low hydrocarbon loading capacity, and cost effectiveness. Despite these, the disadvantages are high energy consumption and high vaporization rate, solvent degradation causing corrosion, foaming, and fouling in vessels and pipelines.[10−12] Ionic liquids are other types of CO_2 absorbents with a low vaporization rate. However, they suffer from a low CO_2 absorption rate, high cost, and high viscosity.[13]

In the past decade, amino acid salt (AAs) aqueous solutions, which are the products of amino acids and alkaline compounds, have shown a superior potential for replacing alkanolamines in CO_2 capture and separation. AAs aqueous solutions have high chemical reactivity due to a higher value of pK_a than that of amine aqueous solutions. Accordingly, the high surface tension of AAs enables them to properly bind to CO_2.[14] They are also more stable against oxidative degradation, with low viscosity and low volatility due to the ionic structure.[11,15] Nonetheless, AAs are more costly and heavier than MEA, which may result in higher absorber size in some high-fraction CO_2 gas streams such as biogas.[16]

Received: December 17, 2020
Accepted: April 2, 2021
Published: May 5, 2021

Few researchers have tried to experimentally measure the equilibrium solubility of CO_2 in AAs aqueous solutions under different operating conditions, CO_2 partial pressures, and absorbent concentrations. In a study, Kang *et al.*[17] reported the solubility of CO_2 in different amino acid-based aqueous solutions. Those compounds were 4 M potassium sarcosinate (K-SAR), a mixture of 1.5 M potassium alaninate and piperazine (K-ALA−PZ), and a mixture of 1.5 M potassium serinate and piperazine (K-SER−PZ) in a temperature range of 313.15−353.15 K. In another study,[18] a solution of potassium prolinate (KPr) mixed with piperazine (PZ) in 1, 4, and 10 wt % concentrations was used to measure the solubility of CO_2, which shows a very high loading capacity. The experimental conditions were ranging at 4.8−2383.2 kPa CO_2 partial pressure and a temperature of 293.15−323.15 K. Both studies concluded that the absorbate solubility decays with an increase in temperature. In some cases, precipitation of AA may occur, which results in shifting the reaction toward products and further CO_2 absorption.[19,20] Kumar *et al.*[19] measured the solubility of CO_2 in potassium taurate aqueous solution in a temperature range of 298−313 K and concentration range of 0.5−4 M. They developed a simple model to interpret the observed crystallization of one of the products during the equilibrium.

Another category of studies focused on measuring the thermophysical properties of AAs to estimate CO_2 absorption. In a study,[21] the thermophysical properties of various AAs aqueous solutions were measured in temperature and concentration ranges of 298−333 K and 0.25−3.5 M, respectively. Using the analogy of N_2O and CO_2 and employing Schumpe's method, CO_2 solubility was estimated based on N_2O solubility measurements. In a similar study, Garcia *et al.*[22] measured viscosity, electrolytic conductivity, density, and the refractive index of potassium for sodium salt aqueous solutions of a-aminobutyric acid at 303.15−343.15 K to correlate these properties under different operating conditions.

As mentioned earlier, limited information is available on the solubility of CO_2 in AAs aqueous solutions under different operating conditions because performing experimental studies is normally time-consuming, expensive, and dangerous in some cases. Moreover, experimental results are normally reported in limited ranges of operating conditions.[23−25] Although models require experimental data for verification and validation, an in-depth understanding and sensitivity analysis of CO_2 and AAs aqueous solution vapor−liquid equilibrium (VLE) require advanced models.

Thermodynamic models utilize different principles to predict/estimate CO_2 solubility in AAs aqueous solutions. For instance, the Kent and Eisenberg[26] model, which is empirical-based, considers non-idealities lumped in equilibrium constants. Another category of models such as Austgen *et al.*,[27] Clegg and Pitzer,[28] the electrolyte−NRTL model of Chen and Evans,[29] and Deshmukh and Mather[30] uses excess Gibbs free energy. Also, there are some equations of state (EoS) that characterize the non-idealities of CO_2 and AAs aqueous solutions VLE. Although these EoS such as SAFT and CPA can reasonably predict/estimate CO_2 solubility in AAs aqueous solutions, they suffer from lack of information available regarding some thermophysical properties of AAs.

Machine learning as a powerful tool can predict/estimate equilibrium properties for CO_2 absorption using measured data.[31−34] To predict/estimate outputs of a regeneration system in a gas sweetening plant, Salooki *et al.*[35] used an artificial neural network (ANN) method. They used some input variables including the inlet temperature of reflux, the difference between inlet and outlet condenser temperatures, and so on to build the ANN. In a similar study,[36] support vector machine (SVM) and ANN methods were compared to estimate the process output variables of the same plant; consequently, the SVM showed a better agreement with experimental data. Accordingly, Ghiasi and Mohammadi[37] used the same tools to predict/estimate the circulation rate of MEA aqueous solution. In another study,[38] an adaptive neuro-fuzzy inference system (ANFIS) was employed to model the CO_2 loading capacity of MEA, DEA, and TEA aqueous solutions used in the CO_2 removal from natural gas streams. The results were significantly improved compared to their previous LSSVM model. As mentioned earlier, the most commonly used machine learning techniques in the literature are the ANN, LSSVM, and ANFIS. A comprehensive review of these methods for modeling of CO_2 equilibrium absorption is given elsewhere.[39]

This study aimed to develop hybrids of machine learning methods (soft computing methods) to model the CO_2 loading capacities of AAs aqueous solutions. For this purpose, we employed least squares support vector machine and coupled simulated annealing optimization algorithm (CSA-LSSVM), radial basis function neural network (RBF-NN), particle swarm optimization−ANFIS (PSO-ANFIS), and hybrid ANFIS models as the machine learning methods.

2. MODEL DEVELOPMENT

2.1. Least Squares Support Vector Machine. One of the most powerful strategies that is frequently used in data mining to process data and recognize patterns is the SVM.[40−42] The SVM builds a function as follows[43]

$$f(x) = w^{\mathrm{T}}\varphi(x) + b \tag{1}$$

in which $\varphi(x)$ is the kernel function, w^{T} represents the transpose of the weight vector of the output layer, and b denotes the bias term. x in this equation stands for the matrix vector with the $N \times n$ dimension, in which N is the number of data points and n represents the number of input parameters to the model. Later on, w^{T} and b need to be optimized *via* the following objective function in eq 2, which should be minimized and is exposed to the subsequent constraints in eq 3[44−46]

$$y_k = w^{\mathrm{T}}\varphi(x_k) + b + e_k \tag{2}$$

$$\begin{aligned} y_k - w^{\mathrm{T}}\varphi(x_k) - b &\le \varepsilon + \xi_k, \qquad k = 1, \ldots, N \\ w^{\mathrm{T}}\varphi(x_k) + b - y_k &\le \varepsilon + \xi_k^*, \qquad k = 1, \ldots, N \\ \xi_k, \xi_k^* &\ge 0, \qquad k = 1, \ldots, N \end{aligned} \tag{3}$$

where x, y, and ε are the input vector, output vector, and fixed precision term of the interpolating function, respectively. ξ_k and ξ_k^* are positive slack terms. The Lagrangian form of this equation can be applied to solve the minimization problem in the previous equation as follows[47]

$$\begin{aligned} L(a, a^*) = -\frac{1}{2}\sum_{k,l=1}^{N}(a_k - a_k^*)(a_1 - a_1^*)K(x_k - x_1) \\ - \varepsilon\sum_{k=1}^{N}(a_k - a_k^*) + \sum_{k=1}^{N} y_k(a_k - a_k^*) \end{aligned} \tag{4}$$

https://doi.org/10.1021/acsomega.0c06158
ACS Omega 2021, 6, 12459−12469

$$\sum_{k=1}^{N} (a_k - a_k^*) = 0,\ a_k,\ a_k^* \in [0,\ c] \tag{5}$$

$$K(x_k - x_1) = \varphi(x_k)^{\mathrm{T}} \varphi(x_1),\ k = 1,\ 2,\ \ldots N \tag{6}$$

a_k and a_k^* denote Lagrangian multipliers in the preceding equations. After applying the Lagrangian multipliers and related constraints, the SVM function of the minimization problem can be expressed as given below[47]

$$f(x) = \sum_{k=1}^{N} (a_k - a_k^*) K(x - x_k) + b \tag{7}$$

in which K represents the Kernel function.

Pelckmans *et al.*[40] introduced a modified version of the SVM, which mathematically solves several linear equations to obtain the best solution. The LSSVM model presents the optimization function and the constraint in eqs 8 and 9 instead of the traditional way of optimizing the error in the SVM[47]

$$\text{cost function} = \frac{1}{2} w^{\mathrm{T}} w + \frac{1}{2} \mu \sum_{k=1}^{n} {e_k}^2 \tag{8}$$

$$y_k = w^{\mathrm{T}} \varphi(x_k) + b + e_k(\text{constraint}) \tag{9}$$

where e_k and μ indicate the error and an tunable variable corresponding to the LSSVM architecture model, respectively. Likewise, the Lagrangian form of the objective function as given below helps us to solve the optimization problem[47]

$$\begin{cases} \dfrac{\partial L}{\partial w} = 0 \rightarrow w = \displaystyle\sum_{k=1}^{n} \alpha_k \varphi(x_k) \\ \dfrac{\partial L}{\partial b} = 0 \rightarrow \displaystyle\sum_{k=1}^{n} \alpha_k = 0 \\ \dfrac{\partial L}{\partial e_k} = 0 \rightarrow \alpha_k = \mu e_k, \qquad k = 1,\ 2,\ \ldots,\ N \\ \dfrac{\partial L}{\partial \alpha_k} = 0 \rightarrow w^{\mathrm{T}} \varnothing(x_k) + b + e_k - y_k = 0, \\ \quad k = 1,\ 2,\ \ldots,\ N \end{cases} \tag{10}$$

By solving the system of equations presented in eq 10, one can obtain the $2N + 2$ equation with $2N + 2$ unknown parameters (α_k, e_k, w, and b). Therefore, the LSSVM variables will be set by solving the abovementioned equations. In this work, we choose the RBF out of existing kernel functions, which is defined as follows[47]

$$K(x,\ x_k) = \exp\left(\frac{\|x_k - x\|^2}{\sigma^2}\right) \tag{11}$$

in which σ^2 suggests the tunable variable of the LSSVM model. These two variables σ^2 and μ can be tuned/adjusted by minimizing the cost function, which is the mean squared error (MSE) of the LSSVM model and actual values as follows[48]

$$\text{MSE} = \frac{\sum_{i=1}^{N} (y_{\text{pred}} - y_{\text{exp}})^2}{N} \tag{12}$$

where y_{pred} denotes the values provided by the LSSVM and y_{exp} represents the experimental data values. In the current study, we used the CSA method introduced by Xavier-de-Souza *et al.*[49] to adjust the value of these parameters. The LSSVM and CSA are normally coupled to reach the best performance in terms of accuracy and reliability.

2.2. Radial Basis Function Neural Network. The RBF neural network is one of the subcategories of the ANN, which can classify the complex systems and specify the type of associated non-linearity with them. The RBF-NN is a three-layer feed-forward network composed of an input, hidden, and output layer.[50] The input layer is responsible for transmitting the input vector to the hidden layer by a transfer function. The number of input nodes in the input layer is equal to the number of input parameters to the model. In the next step, the hidden layer transmits the input data to a higher dimensioned space in the hidden space.[51] All nodes in the hidden layer, unlike other neural networks, are located at a specific point with a particular radius. The amount of space involving the input vector and the center is computed in each neuron.[52] A RBF transfers this calculated space from the hidden layer to the output layer. In the present work, we used the Gaussian transfer function as shown in eq 13 as the basis function of RBF because of a smoother response[53]

$$\varnothing(r) = \exp\left(\frac{r^2}{2\sigma^2}\right) \tag{13}$$

in which r denotes the Euclidean distance between the input vector and RBF and σ is the spread coefficient that represents the smoothness of the interpolation, which is adjusted by users. Ultimately, the output layer linearly sums up all the outputs of the hidden layer as expressed below[53]

$$y_k = \sum_{j=1}^{N} \omega_i \varnothing_{kj}(\|x_k - c_j\|) \tag{14}$$

where $\|x - c\|$ is the Euclidean distance involving the input vector and RBF center, c denotes the RBF center, x represents the input vector, and ω is the weight that connects the nodes. Also, $j = 1, \ldots, N$ where N represents the number of neurons in the hidden layer and $k = 1, \ldots, M$ where M indicates the input vector size.

Two important parameters that determine the performance of the RBF-NN are the spread coefficient and the maximum number of neurons (MNN). Thus, it is critical to assign an optimal value for these parameters to obtain a precise and reliable result from this method.

2.3. Adaptive Neuro-Fuzzy Inference System. The ANFIS combines the principles of the ANN and fuzzy logic to overcome the shortcomings of each model individually.[54] The ANFIS consists of anodes in a five-layer network to build an inference system for predicting/estimating parameters in non-linear systems.[55,56] The fuzzy logic helps us to construct this inference through the training step.[57] The ANFIS utilizes membership functions (MFs) to define each node output O_i^j, in which i is the number of nodes in layer j. The MF for a node is as follows[58]

$$O_i^1 = \mu_{\mathrm{A}_i}(x), \qquad i = 1,\ 2 \tag{15}$$

$$O_i^1 = \mu_{\mathrm{B}_{i-2}}(y), \qquad i = 3,\ 4 \tag{16}$$

where x or y represents the input vector of the node, O_i^1 represents the MF of a fuzzy set (A1, A2, B1, or B2) and it sets the amount that the input vector correlates to the quantifier A, A_i or $\mathrm{B}_{i\text{-}2}$ denotes linguistic label of the adaptive node, and

https://doi.org/10.1021/acsomega.0c06158
ACS Omega 2021, 6, 12459−12469

Table 1. Detail of the Data Used in This Study

AAs	temperature (K)	weight %	CO_2 partial pressure (kPa)	CO_2 loading	ref.
potassium sarcosinate	353.2	50.9	4.6−950.6	0.41−0.83	59
potassium L-asparaginate	313.2−353.2	8.5−34	7.2−951.2	0.17−1.22	59
potassium L-glutaminate	313.2−353.2	9.2−36.8	5.1−871.4	0.28−1.44	59
sodium L-phenylalanine	303.15−333.15	0.1−0.25	1.5−23.11	0.164−1.75	60
sodium glycinate	313.15−333.15	5−25	0.06−773.5	0.0023−1.749	61
potassium lysinate	298.2−353.2	9−41.2	0.47−115.26	0.641−1.781	62
total	**298.2−353.2**	**0.1−50.9**	**0.06−951.2**	**0.0023−1.781**	

μ_{Ai}or $\mu_{Bi\text{-}2}$ is the MF of set A or B. The MF, which is normally generalized bell functions, is as follows[58]

$$\mu_{A_i}(x) = \frac{1}{1 + \left|\left|\frac{x - r_i}{p_i}\right|\right|^{2q_i}} \tag{17}$$

The MF takes a different shape by changing the parameter set p_i, q_i, and r_i. In the second layer, the node function is multiplied by the input signals to produce the output as follows[58]

$$O_i^2 = w_i \mu_{A_i}(x) \mu_{B_i}(y) \qquad i = 1, 2 \tag{18}$$

w_i represents the firing strength. In the next layer, firing strength is normalized by the sum of all firing strengths as follows[58]

$$O_i^3 = \overline{w_i} = \frac{w_i}{w_1 + w_2}, \qquad i = 1, 2 \tag{19}$$

In the fourth layer, each node, using the normalized firing strength $\overline{w}_i$ and parameter set a_i, b_i, and c_i referred to as consequence parameters, computes the output as expressed below[58]

$$O_i^4 = \overline{w_i} z_i = \overline{w_i}(a_i x + b_i y + c_i), \qquad i = 1, 2 \tag{20}$$

In the last layer, the summation of all input signals evaluates the final output as follows[58]

$$O_i^5 = \sum_i \overline{w_i} z_i = \frac{\sum_i w_i z_i}{\sum_i w_i} \tag{21}$$

It is worth noting that in the current study, we used a genetic algorithm (PSO) to find the optimum value for MFs.

3. DEVELOPMENT OF MODELS

In this study, we developed hybrid models to estimate the CO_2 loading capacities of AAs aqueous solutions. The CO_2 loading capacity function is as follows

$$\alpha = f(P_{CO_2}, T, \text{wt \%}, M_{w_{AAs}}, \text{HBD, HBA, RB, HA, complexity}) \tag{22}$$

in which P_{CO2} (kPa) is the CO_2 partial pressure in equilibrium, T (K) represents the temperature, wt % is the mass concentration of the solution, M_{wAAs} (g/mol) denotes the molecular weight of AAs, HBD, HBA, RB, and HA are the hydrogen bond donor count, hydrogen bond acceptor count, rotatable bond count, and heavy atom count, respectively. "Training" and "testing" of the experimental data were randomly chosen with 80−20% ratio with a range presented in Table 1. In order to build up the models, P_{CO2} (kPa), T (K), wt %, M_{wAAs} (g/mol), HBD, HBA, RB, HA, and complexity are regarded as the input parameters and CO_2 loading capacity (α, mole of CO_2 per mole of AAs) is considered as the output parameter. The input and output data are introduced to MATLAB software. The training data set is utilized to train the models, and the test data set is used to evaluate the accuracy of the models. In order to obtain the best LSSVM model, μ and σ^2 should be obtained using the CSA algorithm. In order to find the optimum structure of the ANFIS model, hybrid and PSO algorithms were used. The spread coefficient and the MNN are the key parameters among the other adjusting parameters in the RBF-NN model, which directly affect the model performance. In this work, we employed a trial and error approach to pick optimum values for these parameters. In other words, we defined various RBF-NN structures by adjusting the values for these two variables. These functions then assigned the optimum values to these parameters by minimizing the MSE between the output of the model and the target.

4. RESULTS AND DISCUSSION

As mentioned earlier, the LSSVM model requires the CSA algorithm to calculate the optimum values for μ and σ^2 parameters. These values were calculated as 526.74 and 5.29, respectively.

Because no explicit model was found in the literature to determine the minimum number of MFs,[63,64] we used a trial and error method to estimate it, and Gaussian-type MFs achieved the best result. The ANFIS based on FCM included 14 rules, and the model properties are reported in Table 2. We set the model

Table 2. Developed ANFIS Properties Employed for the Estimation of CO_2 Absorption by AAs Aqueous Solutions

variable	value
fuzzy type	Sugeno-type
initial FIS	Genfis3
MF	Gaussian
output MF	linear
optimization technique	hybrid
no. of fuzzy rules	14
epoch no.	1500

training as 1500 epochs. The model with the minimum test error was selected as the main one. A hybrid learning method was used for parameter estimation. In addition, we employed PSO[65−67] to evaluate the optimal values and train the ANFIS model.

The literature suggests a generalized Gaussian function for the MFs in the fuzzy subdomain.[68−73] Table 3 reports PSO-ANFIS model properties used to estimate CO_2 absorption by the AAs aqueous solutions. The optimum values for the spread coefficient and MNN were obtained as 65 and 195, respectively. Changes in the MSE, which is necessary to track in each step, are shown in Figure 1.

4.1. Model Accuracy and Validation. The models' performance is validated through graphical and statistical

https://doi.org/10.1021/acsomega.0c06158
ACS Omega 2021, 6, 12459−12469

Table 3. Variables in the PSO-ANFIS Model Used for the Estimation of CO_2 Absorption by AAs Aqueous Solutions

parameter	description/value									
Iterations	100	200	500	100	200	500	100	200	500	100
amount of particles	10	10	10	20	20	20	30	30	30	50
initial inertia weight (*W*min)	0.5	0.5	0.5	0.5	0.5	0.5	0.5	0.5	0.5	0.5
inertia weight damping ratio (*W*damp)	0.99	0.99	0.99	0.99	0.99	0.99	0.99	0.99	0.99	0.99
cognitive acceleration (C1)	1	1	1	1	1	1	1	1	1	1
social acceleration (C2)	2	2	2	2	2	2	2	2	2	2
no. of fuzzy rules	10	10	10	10	10	10	10	10	10	10
R^2 (test data)	0.7318	0.7749	0.7459	0.7430	0.7563	0.7706	0.7748	0.7936	0.7886	0.7880
% AARD (test data)	21.54	18.21	20.93	20.05	19.92	17.92	17.50	16.68	18.17	17.20
parameter	**description/value**									
iterations	200	500	100	200	500	100	200	500	200	500
amount of particles	50	50	75	75	75	100	100	100	200	200
initial inertia weight (W_{min})	0.5	0.5	0.5	0.5	0.5	0.5	0.5	0.5	0.5	0.5
inertia weight damping ratio (*W*damp)	0.99	0.99	0.99	0.99	0.99	0.99	0.99	0.99	0.99	0.99
cognitive acceleration (C1)	1	1	1	1	1	1	1	1	1	1
social acceleration (C2)	2	2	2	2	2	2	2	2	2	2
no. of fuzzy rules	10	10	10	10	10	10	10	10	10	10
R^2 (test data)	0.8332	0.8157	0.7522	0.7858	0.8152	0.7903	0.8133	0.8291	0.8877	0.8177
% AARD (test data)	14.40	16.57	17.29	14.49	14.36	16.67	16.41	15.27	11.07	13.22
parameter	**description/value**									
iterations	1000	500	1000	500	800	1000	1200	2000	2000	500
amount of particles	200	150	150	250	250	250	250	250	300	400
initial inertia weight (W_{min})	0.5	0.5	0.5	0.5	0.5	0.5	0.5	0.5	0.5	0.5
inertia Weight Damping Ratio (*W*damp)	0.99	0.99	0.99	0.99	0.99	0.99	0.99	0.99	0.99	0.99
cognitive acceleration (C1)	1	1	1	1	1	1	1	1	1	1
social acceleration (C2)	2	2	2	2	2	2	2	2	2	2
no. of fuzzy rules	10	10	10	10	10	10	10	10	10	10
R^2 (test data)	0.8340	0.7826	0.8432	0.8171	0.8301	0.8769	0.9221	0.8625	0.8697	0.8316
% AARD (test data)	11.81	14.82	12.87	13.82	12.95	10.61	10.00	11.77	11.37	14.02
parameter	**description/value**									
iterations	1000	1200	1200	1200	1200	1200	1200	1200		
amount of particles	400	250	250	250	250	250	250	250		
initial inertia weight (W_{min})	0.5	0.5	0.1	0.7	0.9	0.5	0.5	0.5		
inertia Weight Damping Ratio (*W*damp)	0.99	0.99	0.99	0.99	0.99	0.1	0.5	0.75		
cognitive acceleration (C1)	1	2	1	1	1	1	1	1		
social acceleration (C2)	2	1	2	2	2	2	2	2		
no. of fuzzy rules	10	10	10	10	10	10	10	10		
R^2 (test data)	0.8231	0.7978	0.9160	0.8137	0.9103	0.9182	0.9293	0.8395		
% AARD (test data)	10.56	17.54	11.79	13.45	9.446	9.750	7.661	13.75		

methods. Figure 2 compares the values estimated by the model against the experimental data used in this work. The correlation coefficients of the regression line for the RBF-NN are higher than those of the other models, and the best fit line significantly lies over the 45° line, indicating a good agreement between model results and real measurements. Considering the correlation coefficient of 0.9752 for the RBF-NN, the model output displays a superior fit with actual data. Figure 3 illustrates the consistency of models' output *versus* the experimental data in terms of relative deviation for absorption of CO_2 by the solutions. According to Figure 3, the maximum relative deviations for the CSA-LSSVM, RBF-NN, PSO-ANFIS, and hybrid ANFIS are 1.54, 6.66, 21.21, and 21.62, respectively.

Obviously, the lowest relative deviation belongs to the PSO-ANFIS because the relative error of this model lies in the range of 0−0.3. Figure 4 depicts the model estimations *versus* the actual data point index to gain a realistic sense of model precision; the result indicates a good fit between model results and real measurements.

Four additional data analysis parameters including the correlation factor (R^2), average absolute relative deviation (AARD), standard deviation (STD), and root mean squared error (RMSE) are shown in Table 4 to demonstrate the models' performances. In the following equations, x stands for the CO_2 absorption[56]

$$R^2 = 1 - \frac{\sum_{i=1}^{n} [x_i^{\text{estimated}} - x_i^{\text{experimental}}]^2}{\sum_{i=1}^{n} [x_i^{\text{estimated}} - x^m]^2},\ x_m = \frac{\sum_{i=1}^{n} x_i^{\text{experimental}}}{n} \tag{23}$$

$$\%\text{AARD} = \frac{100}{n} \sum_{i=1}^{n} \frac{|x_i^{\text{estimated}} - x_i^{\text{experimental}}|}{x_i^{\text{exp}}} \tag{24}$$

$$\text{MSE} = \frac{1}{n} \sum_{i=1}^{n} (x_i^{\text{experimental}} - x_i^{\text{estimated}})^2 \tag{25}$$

https://doi.org/10.1021/acsomega.0c06158
ACS Omega 2021, 6, 12459−12469

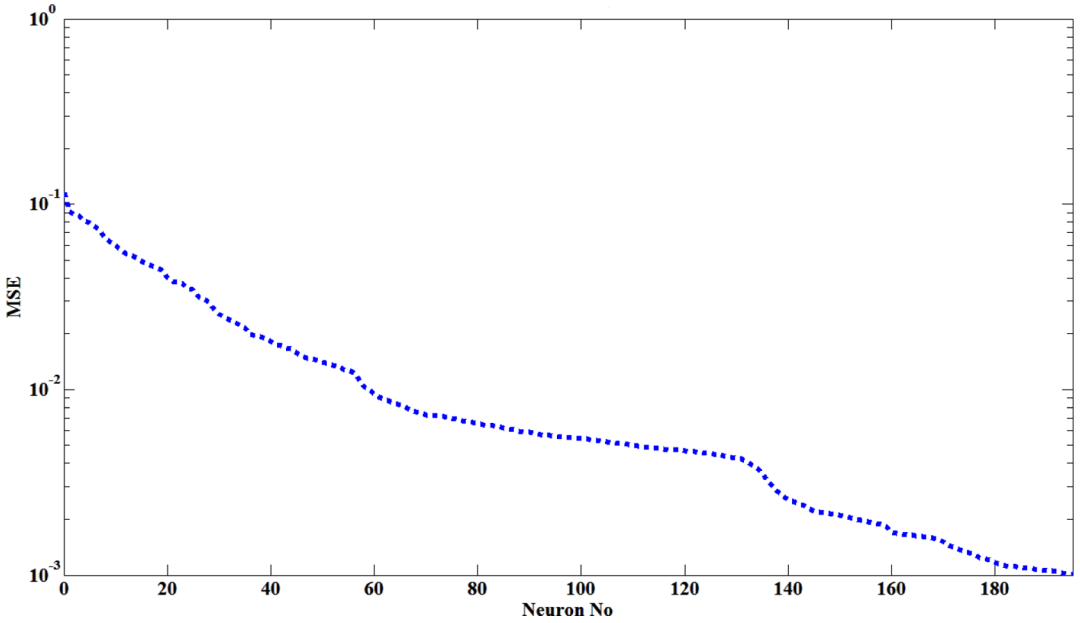

Figure 1. Convergence of the RBF-NN to the best structure.

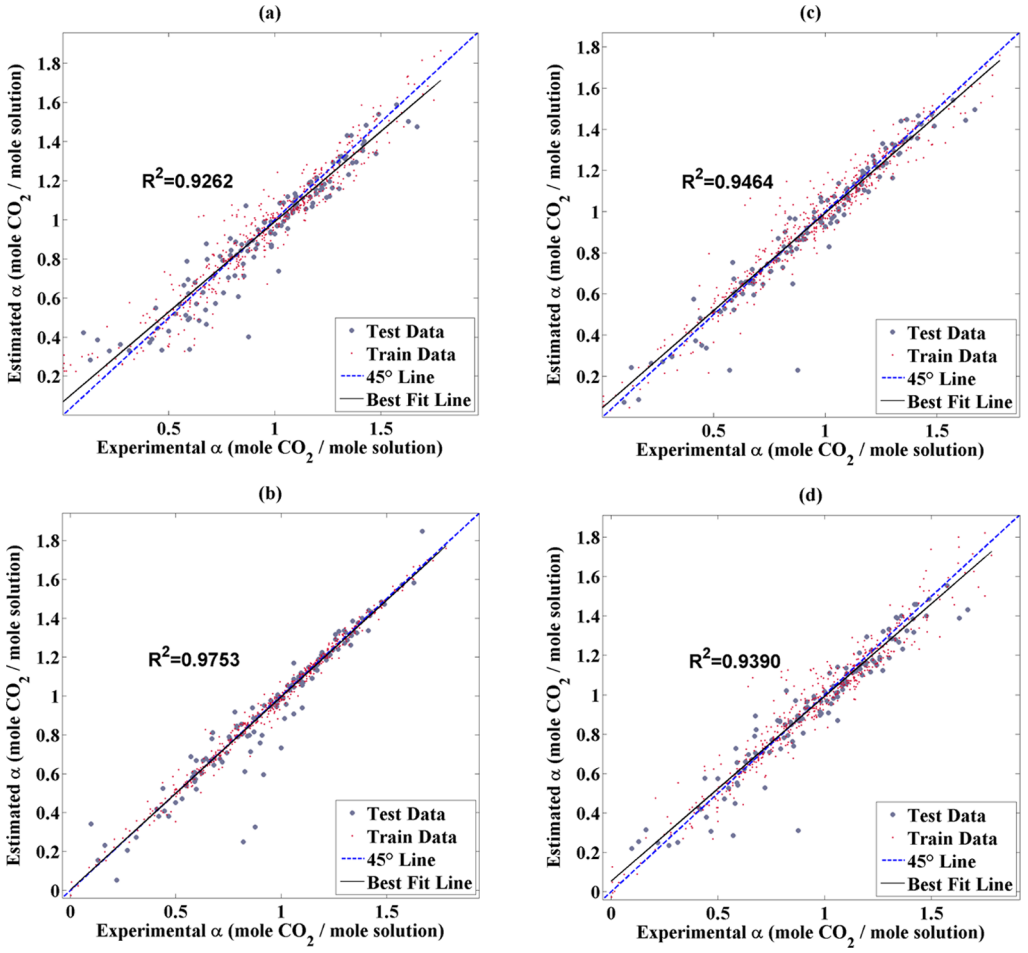

Figure 2. Regression plot for the absorption of CO_2 prognostication by (a) LSSVM, (b) RBF-NN, (c) PSO-ANFIS, and (d) ANFIS.

$$\mathrm{STD} = \sqrt{\sum_{i=1}^{n}\left(\frac{(x_i^{\text{estimated}} - x_m)^2}{n}\right)} \tag{26}$$

The RBF-NN model results in a higher correlation coefficient and lower MSE, AARD %, and STD, which conveys a more promising performance for this model against other models. Table 5 demonstrates the % AARD, which is estimated by the

https://doi.org/10.1021/acsomega.0c06158
ACS Omega 2021, 6, 12459−12469

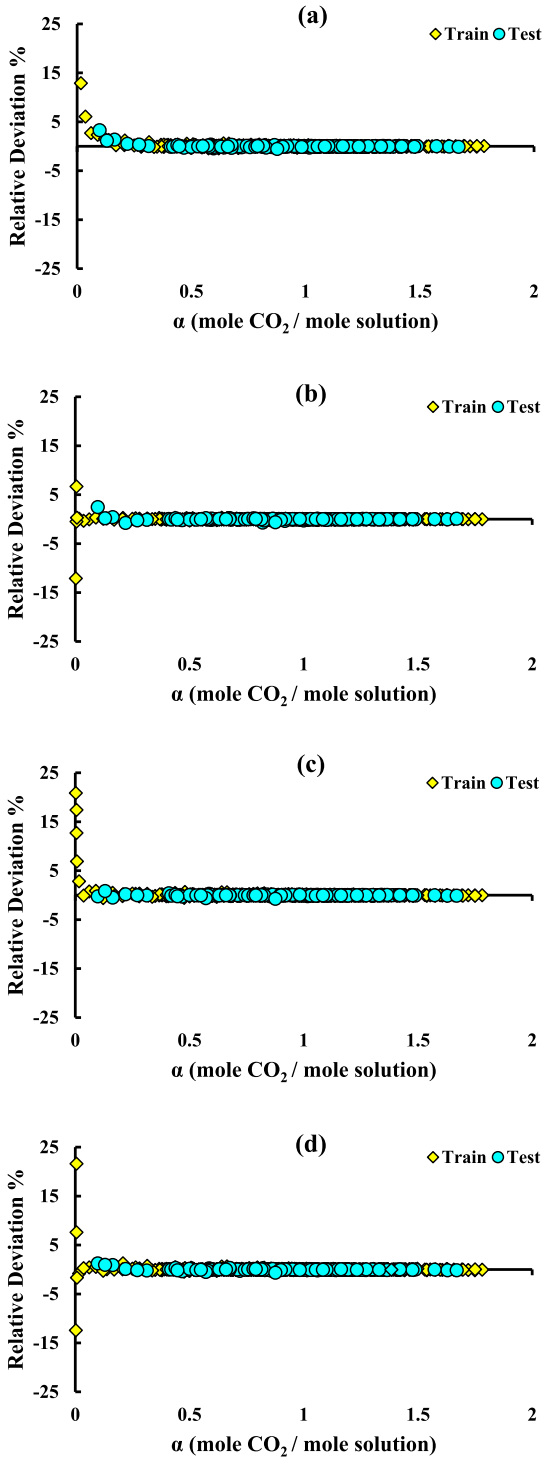

Figure 3. Relative deviation of the estimated CO_2 absorption values for both test and train data points by (a) LSSVM, (b) RBF-NN, (c) PSO-ANFIS, and (d) ANFIS.

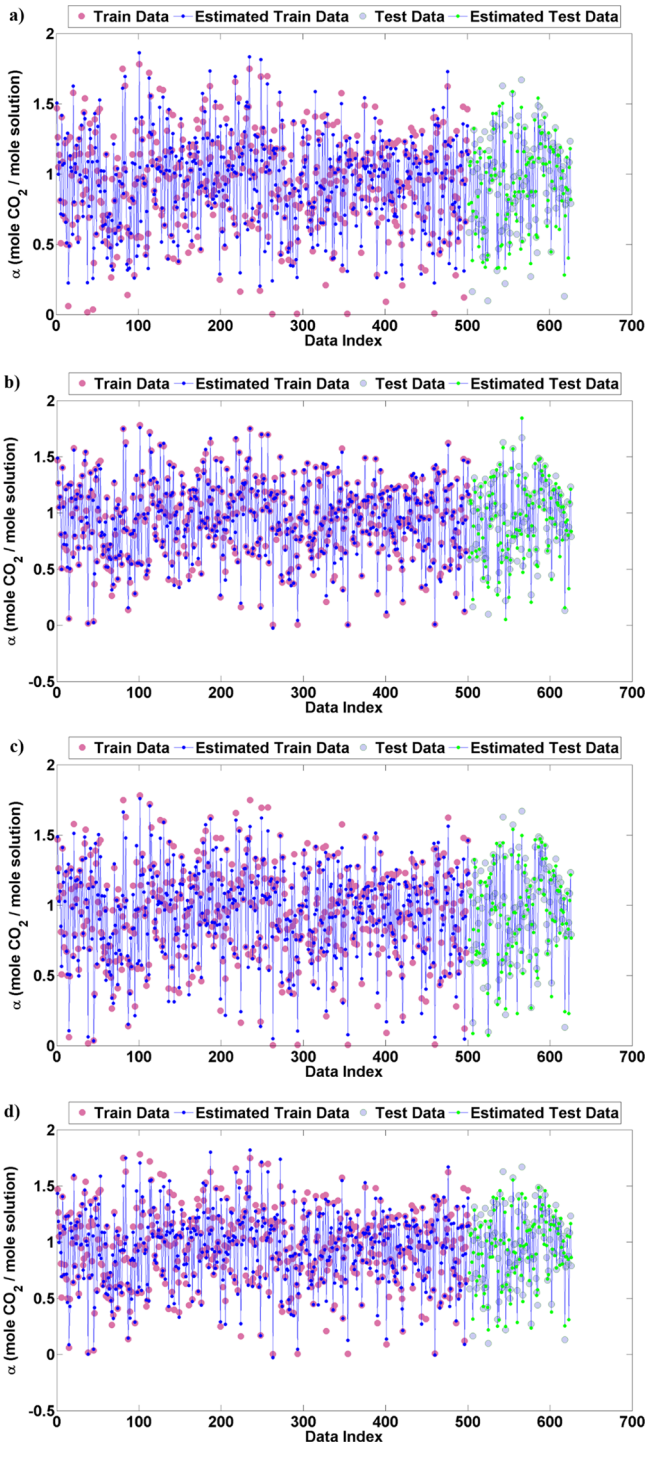

Figure 4. Actual CO_2 absorption *versus* estimated data at testing and training stages for (a) LSSVM, (b) RBF-NN, (c) PSO-ANFIS, and (d) ANFIS.

developed models. As can be seen, except in the case of potassium L-asparaginate that the ANFIS AARD is lower than other models' AARDs, the RBF-NN AARD is lower than other models' AARD in other cases.

Accordingly, Figure 5 provides a more clear picture to evaluate the aforementioned parameters and endorses the excellence of the RBF-NN in estimating the CO_2 absorption compared to other models.

Figures 6 and 7 demonstrate the impact of pressure at various temperatures and concentrations of aqueous sodium L-phenylalanine (Na-Phe) solution. According to these figures at a given temperature and concentration, CO_2 absorption increases as the CO_2 pressure rises, which directly affects the CO_2 loading. The reason is that an increase in pressure reproduces the collision of gas molecules on the solution surface, which subsequently helps CO_2 molecules diffuse into the solution to a greater extent.[74] Figure 6 shows the effect of temperature on the loading. Since

https://doi.org/10.1021/acsomega.0c06158
ACS Omega 2021, 6, 12459−12469

Table 4. Accuracies of Different Models

model	parameter		
	train	test	total
	LSSVM		
R^2	0.9326	0.9036	0.9262
MSE	0.0078	0.0111	0.0085
STD	0.3263	0.3170	0.3244
% AARD	59.40	13.45	50.23
	RBF-NN		
R^2	0.9913	0.9155	0.9753
MSE	0.0010	0.0103	0.0028
STD	0.3390	0.3450	0.3402
% AARD	6.86	9.33	7.350
	PSO-ANFIS		
R^2	0.9519	0.9293	0.9464
MSE	0.0056	0.0084	0.0061
STD	0.3285	0.3354	0.3298
% AARD	19.07	7.66	16.79
	ANFIS		
R^2	0.9451	0.9157	0.9390
MSE	0.0064	0.0095	0.0070
STD	0.3310	0.3176	0.3283
% AARD	15.76	10.09	14.63

Table 5. % AARD for Each AAs Aqueous Solution Estimated by the Developed Model

AAs	% AARD				no. data
	LSSVM	RBF-NN	PSO-ANFIS	ANFIS	
potassium sarcosinate	4.20	0.427	7.95	3.64	12
potassium L-asparaginate	5.59	4.23	6.48	3.88	91
potassium L-glutaminate	6.11	2.87	5.17	3.90	100
sodium L-phenylalanine	16.90	6.43	10.56	15.89	63
sodium glycinate	226.1	24.44	17.50	47.71	123
potassium lysinate	5.88	1.88	5.17	6.25	237
total	**50.23**	**7.35**	**16.79**	**14.63**	**626**

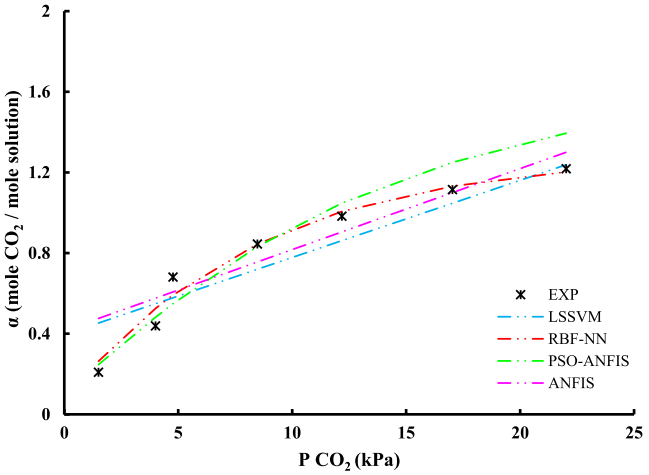

Figure 5. Absorption of CO_2 by an aqueous solution of 0.25 wt % sodium L-phenylalanine at 313.15 K. Experimental data.[60]

the absorption is an exothermic process, as per Le Chaterlier's principle, an increase in temperature results in a decrease in CO_2 absorption.[75] Therefore, temperature impacts CO_2 solubility conversely. Accordingly, as Figure 7 depicts, CO_2 loading decreases as Na-Phe concentration increases in the solution. CO_2 loading is defined as the absorbed moles of CO_2 per mole of AAs in the solution. Consequently, because Na-Phe moles increase more rapidly compared with absorbed CO_2 moles, the CO_2 loading declines as Na-Phe concentration increases.[60]

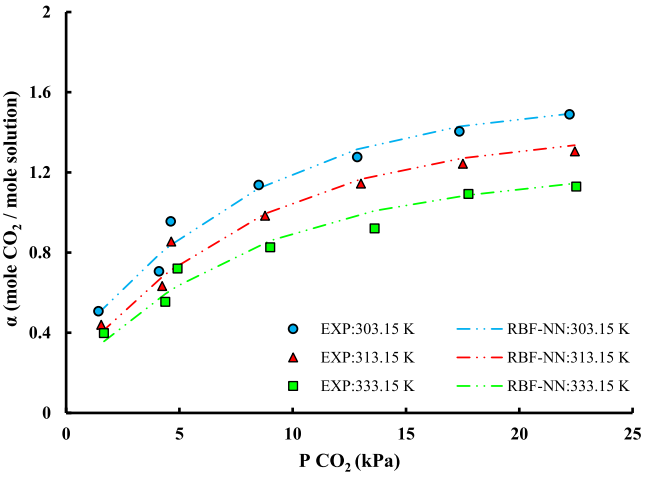

Figure 6. Absorption of CO_2 by an aqueous solution of 0.2 wt % sodium L-phenylalanine at different temperatures. Experimental data.[60]

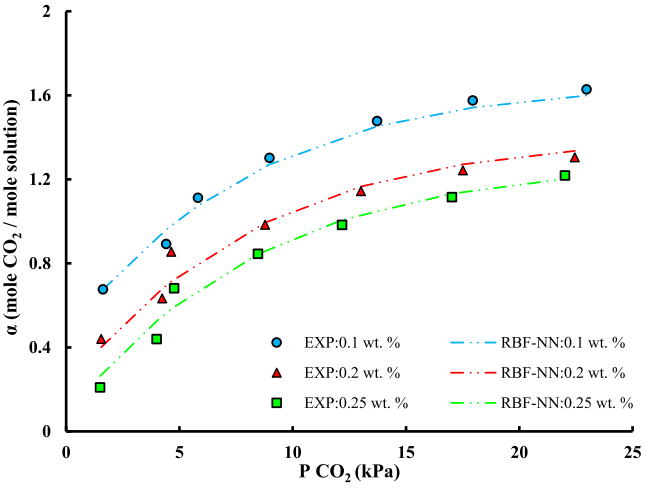

Figure 7. Absorption of CO_2 by different aqueous solutions of sodium L-phenylalanine solution at 313.15 K. Experimental data.[60]

4.2. Sensitivity Analysis. To investigate the effects of input parameters on the CO_2 and AAs aqueous solution equilibrium, a sensitivity analysis was performed. The relevancy factor (r) with directionality in Pearson correlation helps us to gain a clearer understanding of the input parameter influences on the system as follows[76,77]

$$r(V_j, \text{loading}) = \frac{\sum_{i=1}^{n}(V_{j,i} - \overline{V_j})(L_i - \overline{L})}{\sqrt{\sum_{i=1}^{n}(V_{j,i} - \overline{V_j})^2 \sum_{i=1}^{n}(L_i - \overline{L})^2}} \quad (27)$$

in which L_i and $\overline{L}$ denote the ith and the average values of CO_2 loading, respectively, and $V_{j,i}$ and $\overline{V_j}$ represent the ith and average values of the jth input variable, respectively. The relevancy factor ranges from −1 to 1, where a negative value indicates a decreasing correlation between the input variables and the

https://doi.org/10.1021/acsomega.0c06158
ACS Omega 2021, 6, 12459−12469

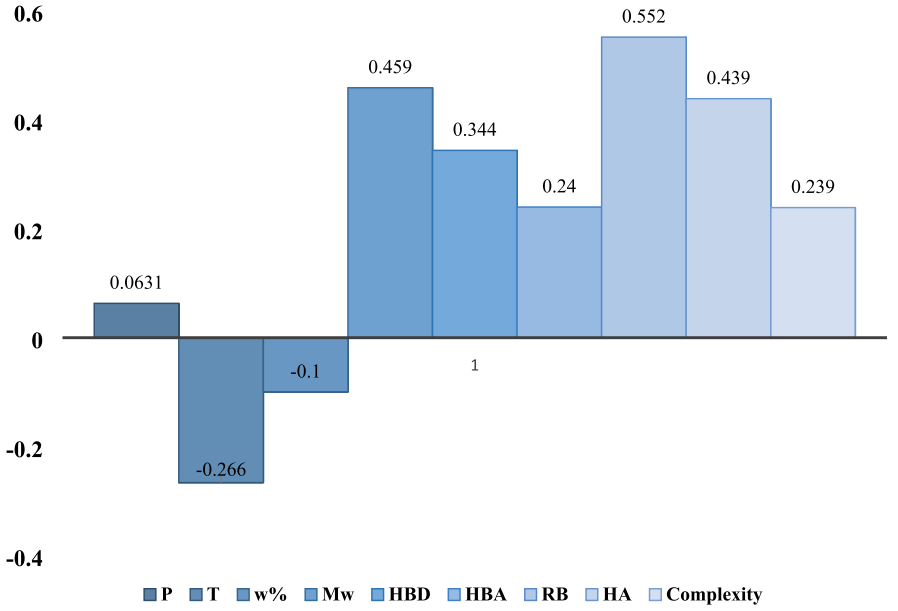

Figure 8. Sensitivity analysis of the RBF-NN model.

loading, a positive value indicates the opposite, and zero means no correlation. Figure 8 clearly illustrates that the RB value impacts the loading the most with an increasing correlation. The molecular weight (M_w) of the AAs is the second noticeable factor that raises the loading as it increases. Moreover, there are two other parameters that slightly influence CO_2 loading. Temperature and amine concentration have a negative effect on the loading.

5. CONCLUSIONS

Four hybrid machine learning models were developed to estimate CO_2 loading capacities of AAs aqueous solutions, namely, potassium sarcosinate, potassium L-asparaginate, potassium L-glutaminate, sodium L-phenylalanine, sodium glycinate, and potassium lysinate as a function of temperature, mass concentration of AAs in the aqueous solution, molecular weight of AAs, HBD, HBA, RB, HA, and complexity. The four methods are the CSA-LSSVM, RBF-NN, PSO-ANFIS, and hybrid ANFIS, among which the RBF-NN outperformed other methods in estimating the CO_2 loading capacities of AAs aqueous solutions. The AARD %s of the model results and actual data are 13.4, 9.3, 7.6, and 10 for CSA-LSSVM, RBF-NN, PSO-ANFIS, and hybrid ANFIS models, respectively. For training and testing, experimental data points covering different AAs aqueous solutions and gathered from reliable references were utilized. The RBF-NN could estimate the CO_2 loading capacities of AAs aqueous solutions with acceptable accuracy.

AUTHOR INFORMATION

Corresponding Authors

Amir Dashti − *Department of Chemical Engineering, Faculty of Engineering, University of Kashan, Kashan 8731753153, Iran;* orcid.org/0000-0002-3937-7353; Email: amirdashti13681990@gmail.com

Amir H. Mohammadi − *Discipline of Chemical Engineering, School of Engineering, University of KwaZulu-Natal, Durban 4041, South Africa;* orcid.org/0000-0002-2947-1135; Email: amir_h_mohammadi@yahoo.com

Authors

Farid Amirkhani − *Department of Chemical Engineering, Faculty of Engineering, University of Kashan, Kashan 8731753153, Iran*

Amir-Sina Hamedi − *Department of Chemical Engineering, Brigham Young University, Provo, Utah 84602, United States*

Complete contact information is available at: https://pubs.acs.org/10.1021/acsomega.0c06158

Notes

The authors declare no competing financial interest.

REFERENCES

(1) Altamash, T.; Nasser, M. S.; Elhamarnah, Y.; Magzoub, M.; Ullah, R.; Qiblawey, H.; Aparicio, S.; Atilhan, M. Gas solubility and rheological behavior study of betaine and alanine based natural deep eutectic solvents (NADES). *J. Mol. Liq.* **2018**, *256*, 286−295.

(2) Zarei, A.; Hafizi, A.; Rahimpour, M. R.; Raeissi, S. Carbon dioxide absorption into aqueous potassium salt solutions of glutamine amino acid. *J. Mol. Liq.* **2020**, *301*, 111743.

(3) Safdar, R.; Omar, A. A.; Lal, B. Performance of aqueous tetrabutylammonium hydroxide, piperazine and their blends for carbon dioxide capture. *J. Mol. Liq.* **2018**, *266*, 522−528.

(4) Borhani, T. N.; Wang, M. Role of solvents in CO_2 capture processes: The review of selection and design methods. *Renewable Sustainable Energy Rev.* **2019**, *114*, 109299.

(5) Amirkhani, F.; Harami, H. R.; Asghari, M. CO_2/CH_4 mixed gas separation using poly (ether-b-amide)-ZnO nanocomposite membranes: Experimental and molecular dynamics study. *Polym. Test.* **2020**, *86*, 106464.

(6) Amirkhani, F.; Mosadegh, M.; Asghari, M.; Parnian, M. J. The beneficial impacts of functional groups of CNT on structure and gas separation properties of PEBA mixed matrix membranes. *Polym. Test.* **2020**, *82*, 106285.

(7) Mosadegh, M.; Amirkhani, F.; Riasat Harami, H.; Asghari, M.; Parnian, M. J. Effect of Nafion and APTEOS functionalization on mixed gas separation of PEBA-FAU membranes: experimental study and MD and GCMC simulations. *Sep. Purif. Technol.* **2020**, *247*, 116981.

(8) Guo, Y.; Tan, C.; Sun, J.; Li, W.; Zhang, J.; Zhao, C. Porous activated carbons derived from waste sugarcane bagasse for CO_2 adsorption. *Chem. Eng. J.* **2020**, *381*, 122736.

(9) Yan, H.; Zhao, L.; Bai, Y.; Li, F.; Dong, H.; Wang, H.; Zhang, X.; Zeng, S. Superbase ionic liquid-based deep eutectic solvents for improving CO_2 absorption. *ACS Sustainable Chem. Eng.* **2020**, *8*, 2523−2530.
(10) Ma'mun, S.; Nilsen, R.; Svendsen, H. F.; Juliussen, O. Solubility of carbon dioxide in 30 mass% monoethanolamine and 50 mass% methyldiethanolamine solutions. *J. Chem. Eng. Data* **2005**, *50*, 630−634.
(11) Ramezani, R.; Mazinani, S.; Di Felice, R. State-of-the-art of CO_2 capture with amino acid salt solutions. *Rev. Chem. Eng.* **2020**, 385.
(12) Xu, X.; Myers, M. B.; Versteeg, F. G.; Adam, E.; White, C.; Crooke, E.; Wood, C. D. Next generation amino acid technology for CO_2 capture. *J. Mater. Chem. A.* **2021**, *9*, 1692.
(13) Kenarsari, S. D.; Yang, D.; Jiang, G.; Zhang, S.; Wang, J.; Russell, A. G.; Wei, Q.; Fan, M. Review of recent advances in carbon dioxide separation and capture. *RSC Adv.* **2013**, *3*, 22739−22773.
(14) Kumar, P. S.; Hogendoorn, J. A.; Feron, P. H. M.; Versteeg, G. F., Density, viscosity, solubility, and diffusivity of N_2O in aqueous amino acid salt solutions. **2001**, *46* (), 1357-1361. DOI: 10.1021/je010043a
(15) Payagala, T.; Armstrong, D. W. Chiral ionic liquids: A compendium of syntheses and applications (2005-2012). *J. Chem. Eng. Data* **2012**, *24*, 17−53.
(16) Abdeen, F. R. H.; Mel, M.; Jami, M. S.; Ihsan, S. I.; Ismail, A. F. A review of chemical absorption of carbon dioxide for biogas upgrading. *Chin. J. Chem. Eng.* **2016**, *24*, 693−702.
(17) Kang, D.; Park, S.; Jo, H.; Min, J.; Park, J. Solubility of CO_2 in amino-acid-based solutions of (potassium sarcosinate),(potassium alaninate+ piperazine), and (potassium serinate+ piperazine). *J. Chem. Eng. Data* **2013**, *58*, 1787−1791.
(18) Hamzehie, M. E.; Najibi, H. Carbon dioxide loading capacity in aqueous solution of Potassium salt of Proline blended with Piperazine as new absorbents. *Thermochim. Acta* **2016**, *639*, 66−75.
(19) Kumar, P. S.; Hogendoorn, J. A.; Timmer, S. J.; Feron, P. H. M.; Versteeg, G. F. Equilibrium solubility of CO_2 in aqueous potassium taurate solutions: Part 2. Experimental VLE data and model. *Ind. Eng. Chem. Res.* **2003**, *42*, 2841−2852.
(20) Rezakazemi, M.; Niazi, Z.; Mirfendereski, M.; Shirazian, S.; Mohammadi, T.; Pak, A. CFD simulation of natural gas sweetening in a gas-liquid hollow-fiber membrane contactor. *Chem. Eng. J.* **2011**, *168*, 1217−1226.
(21) Holst, J. v.; Kersten, S. R. A.; Hogendoorn, K. J. A. Physiochemical properties of several aqueous potassium amino acid salts. *J. Chem. Eng. Data* **2008**, *53*, 1286−1291.
(22) Garcia, A. A. R.; Leron, R. B.; Soriano, A. N.; Li, M.-H. Thermophysical property characterization of aqueous amino acid salt solutions containing α -aminobutyric acid. *J. Chem. Thermodyn.* **2015**, *81*, 136−142.
(23) Mazinani, S.; Ramazani, R.; Samsami, A.; Jahanmiri, A.; Van der Bruggen, B.; Darvishmanesh, S. Equilibrium solubility, density, viscosity and corrosion rate of carbon dioxide in potassium lysinate solution. *Fluid Phase Equilib.* **2015**, *396*, 28−34.
(24) Shen, S.; Yang, Y.-n.; Wang, Y.; Ren, S.; Han, J.; Chen, A. CO_2 absorption into aqueous potassium salts of lysine and proline: Density, viscosity and solubility of CO_2. *Fluid Phase Equilib.* **2015**, *399*, 40−49.
(25) Ramazani, R.; Samsami, A.; Jahanmiri, A.; Bruggen, B. V. d.; Mazinani, S. Characterization of monoethanolamine + potassium lysinate blend solution as a new chemical absorbent for CO_2 capture. *Int. J. Greenhouse Gas Control* **2016**, *51*, 29−35.
(26) Kent, R.; Eisenberg, B. *Gas conditioning Conference*; University of Oklahoma, 1975. Also, 1976; Vol. *55* (2); p 87.
(27) Austgen, D. M.; Rochelle, G. T.; Peng, X.; Chen, C. C. Model of vapor-liquid equilibria for aqueous acid gas-alkanolamine systems using the electrolyte-NRTL equation. *Ind. Eng. Chem. Res.* **1989**, *28*, 1060−1073.
(28) Clegg, S. L.; Pitzer, K. S. Thermodynamics of multicomponent, miscible, ionic solutions: generalized equations for symmetrical electrolytes. *J. Phys. Chem.* **1992**, *96*, 3513−3520.
(29) Chen, C.-C.; Evans, L. B. A local composition model for the excess Gibbs energy of aqueous electrolyte systems. *AIChE J.* **1986**, *32*, 444−454.
(30) Deshmukh, R. D.; Mather, A. E. A mathematical model for equilibrium solubility of hydrogen sulfide and carbon dioxide in aqueous alkanolamine solutions. *Chem. Eng. Sci.* **1981**, *36*, 355−362.
(31) Razavi, R.; Bemani, A.; Baghban, A.; Mohammadi, A. H. Modeling of CO_2 absorption capabilities of amino acid solutions using a computational scheme. *Environ. Prog. Sustainable Energy* **2020**, *39*, No. e13430.
(32) Liu, Z.; Li, H.; Liu, K.; Yu, H.; Cheng, K. Design of high-performance water-in-glass evacuated tube solar water heaters by a high-throughput screening based on machine learning: A combined modeling and experimental study. *Sol. Energy* **2017**, *142*, 61−67.
(33) Li, H.; Liu, Z.; Liu, K.; Zhang, Z. Predictive power of machine learning for optimizing solar water heater performance: the potential application of high-throughput screening. *Int. J. Photoenergy* **2017**, *2017*, 4194251.
(34) Li, H.; Tang, X.; Wang, R.; Lin, F.; Liu, Z.; Cheng, K. Comparative Study on Theoretical and Machine Learning Methods for Acquiring Compressed Liquid Densities of 1,1,1,2,3,3,3-Heptafluoropropane (R227ea) via Song and Mason Equation, Support Vector Machine, and Artificial Neural Networks. *Appl. Sci.* **2016**, *6*, 25.
(35) Salooki, M. K.; Abedini, R.; Adib, H.; Koolivand, H. Design of neural network for manipulating gas refinery sweetening regenerator column outputs. *Sep. Purif. Technol.* **2011**, *82*, 1−9.
(36) Adib, H.; Sharifi, F.; Mehranbod, N.; Kazerooni, N. M.; Koolivand, M. Support Vector Machine based modeling of an industrial natural gas sweetening plant. *J. Nat. Gas Sci. Eng.* **2013**, *14*, 121−131.
(37) Ghiasi, M. M.; Mohammadi, A. Development of reliable models for determination of required monoethanolamine (MEA) circulation rate in amine plants. *Sep. Sci. Technol.* **2015**, *50*, 2248−2256.
(38) Ghiasi, M. M.; Arabloo, M.; Mohammadi, A. H.; Barghi, T. Application of ANFIS soft computing technique in modeling the CO_2 capture with MEA, DEA, and TEA aqueous solutions. *Int. J. Greenhouse Gas Control* **2016**, *49*, 47−54.
(39) Dashti, A.; Raji, M.; Alivand, M. S.; Mohammadi, A. H. Estimation of CO_2 equilibrium absorption in aqueous solutions of commonly used amines using different computational schemes. *Fuel* **2020**, *264*, 116616.
(40) Pelckmans, K.; Suykens, J. A.; Van Gestel, T.; De Brabanter, J.; Lukas, L.; Hamers, B.; De Moor, B.; Vandewalle, J. *LS-SVMlab: a matlab/c Toolbox for Least Squares Support Vector Machines*; ESAT-SCD-SISTA K.U. Leuve, 2002; Vol. *142*; pp 1−2.
(41) Gharagheizi, F.; Eslamimanesh, A.; Farjood, F.; Mohammadi, A. H.; Richon, D. Solubility Parameters of Nonelectrolyte Organic Compounds: Determination Using Quantitative Structure-Property Relationship Strategy. *Ind. Eng. Chem. Res.* **2011**, *50*, 11382−11395.
(42) Dashti, A.; Mazaheri, O.; Amirkhani, F.; Mohammadi, A. H. Molecular descriptors-based models for estimating net heat of combustion of chemical compounds. *Energy* **2021**, *217*, 119292.
(43) Suykens, J. A.; Van Gestel, T.; De Brabanter, J. *Least squares support vector machines*; World scientific, 2002.
(44) Eslamimanesh, A.; Gharagheizi, F.; Illbeigi, M.; Mohammadi, A. H.; Fazlali, A.; Richon, D. Phase equilibrium modeling of clathrate hydrates of methane, carbon dioxide, nitrogen, and hydrogen+water soluble organic promoters using Support Vector Machine algorithm. *Fluid Phase Equilib.* **2012**, *316*, 34−45.
(45) Agarwal, S.; Vijaya Saradhi, V.; Karnick, H., Kernel-based online machine learning and support vector reduction. **2008**, *71* (), 1230-1237. DOI: 10.1016/j.neucom.2007.11.023
(46) Zhao, C.; Zhang, H.; Zhang, X.; Liu, M.; Hu, Z.; Fan, B. Application of support vector machine (SVM) for prediction toxic activity of different data sets. *Toxicology* **2006**, *217*, 105−119.
(47) Barati-Harooni, A.; Najafi-Marghmaleki, A.; Arabloo, M.; Mohammadi, A. H. Chemical structural models for prediction of heat capacities of ionic liquids. *J. Mol. Liq.* **2017**, *232*, 113−122.
(48) Dashti, A.; Amirkhani, F.; Jokar, M.; Mohammadi, A. H.; Chau, K.-W. Insights into the estimation of heavy metals ions sorption from

aqueous environment onto natural zeolite. *Int. J. Environ. Sci. Technol.* **2020**..
(49) Xavier-de-Souza, S.; Suykens, J. A.; Vandewalle, J.; Bollé, D. Coupled simulated annealing. *Int. J. Environ. Sci. Technol.* **2009**, *40*, 320−335.
(50) Panda, S. S.; Chakraborty, D.; Pal, S. K. Flank wear prediction in drilling using back propagation neural network and radial basis function network. *Appl. Soft Comput.* **2008**, *8*, 858−871.
(51) Zhao, N.; Wen, X.; Yang, J.; Li, S.; Wang, Z. Modeling and prediction of viscosity of water-based nanofluids by radial basis function neural networks. *Powder Technol.* **2015**, *281*, 173−183.
(52) Yu, L.; Lai, K. K.; Wang, S. Multistage RBF neural network ensemble learning for exchange rates forecasting. *Neurocomputing* **2008**, *71*, 3295−3302.
(53) Varamesh, A.; Hemmati-Sarapardeh, A.; Dabir, B.; Mohammadi, A. H. Development of robust generalized models for estimating the normal boiling points of pure chemical compounds. *J. Mol. Liq.* **2017**, *242*, 59−69.
(54) Jang, J.-S. R. ANFIS: adaptive-network-based fuzzy inference system. *IEEE Trans. Syst. Man Cybern. Syst.* **1993**, *23*, 665−685.
(55) Dashti, A.; Jokar, M.; Amirkhani, F.; Mohammadi, A. H. Quantitative structure property relationship schemes for estimation of autoignition temperatures of organic compounds. *J. Mol. Liq.* **2020**, *300*, 111797.
(56) Dashti, A.; Bahrololoomi, A.; Amirkhani, F.; Mohammadi, A. H. Estimation of CO_2 adsorption in high capacity metal− organic frameworks: Applications to greenhouse gas control. *J. CO2 Util.* **2020**, *41*, 101256.
(57) Yun, Z.; Quan, Z.; Caixin, S.; Shaolan, L.; Yuming, L.; Yang, S. RBF neural network and ANFIS-based short-term load forecasting approach in real-time price environment. *IEEE Trans. Power Syst.* **2008**, *23*, 853−858.
(58) Ying, L.-C.; Pan, M.-C. Using adaptive network based fuzzy inference system to forecast regional electricity loads. *Energy Convers. Manage.* **2008**, *49*, 205−211.
(59) Chen, Z.-W.; Leron, R. B.; Li, M.-H. Equilibrium solubility of carbon dioxide in aqueous potassium L-asparaginate and potassium L-glutaminate solutions. *Fluid Phase Equilib.* **2015**, *400*, 20−26.
(60) Garg, S.; Shariff, A. M.; Shaikh, M. S.; Lal, B.; Suleman, H.; Faiqa, N. thermodynamic and neural network modeling of CO_2 solubility in aqueous sodium salt of l-phenylalanine. *J. CO2 Util.* **2017**, *19*, 146−156.
(61) Mondal, B. K.; Bandyopadhyay, S. S.; Samanta, A. N. VLE of CO_2 in aqueous sodium glycinate solution−New data and modeling using Kent−Eisenberg model. *Int. J. Greenhouse Gas Control* **2015**, *36*, 153−160.
(62) Shen, S.; Zhao, Y.; Bian, Y.; Wang, Y.; Guo, H.; Li, H. CO_2 absorption using aqueous potassium lysinate solutions: vapor−liquid equilibrium data and modelling. *J. Chem. Thermodyn.* **2017**, *115*, 209−220.
(63) Rezakazemi, M.; Ghafarinazari, A.; Shirazian, S.; Khoshsima, A. Numerical modeling and optimization of wastewater treatment using porous polymeric membranes. *Polym. Eng. Sci.* **2013**, *53*, 1272−1278.
(64) Yingjie, L.; Baoshu, W. Study on the control course of ANFIS based aircraft auto-landing. *J. Electr. Electron. Eng.* **2005**, *16*, 583−587.
(65) Dashti, A.; Riasat Harami, H.; Rezakazemi, M.; Shirazian, S. Estimating CH4 and CO2 solubilities in ionic liquids using computational intelligence approaches. *J. Mol. Liq.* **2018**, *271*, 661−669.
(66) Rezakazemi, M.; Dashti, A.; Asghari, M.; Shirazian, S. H_2-selective mixed matrix membranes modeling using ANFIS, PSO-ANFIS, GA-ANFIS. *Int. J. Hydrogen Energy* **2017**, *42*, 15211−15225.
(67) Dashti, A.; Raji, M.; Azarafza, A.; Baghban, A.; Mohammadi, A. H.; Asghari, M. Rigorous prognostication and modeling of gas adsorption on activated carbon and Zeolite-5A. *J. Environ. Manage.* **2018**, *224*, 58−68.
(68) Ganjidoost, H.; Mousavi, S. J.; Soroush, A. Adaptive network-based fuzzy inference systems coupled with genetic algorithms for predicting soil permeability coefficient. *Neural Process. Lett.* **2016**, *44*, 53−79.
(69) Ghasemi, E.; Kalhori, H.; Bagherpour, R. A new hybrid ANFIS-PSO model for prediction of peak particle velocity due to bench blasting. *Eng. Comput.* **2016**, *32*, 607−614.
(70) Hasanipanah, M.; Amnieh, H. B.; Arab, H.; Zamzam, M. S. Feasibility of PSO−ANFIS model to estimate rock fragmentation produced by mine blasting. *Neural. Comput. Appl.* **2018**, *30*, 1015−1024.
(71) Tatar, A.; Barati-Harooni, A.; Najafi-Marghmaleki, A.; Mohebbi, A.; Ghiasi, M. M.; Mohammadi, A. H.; Hajinezhad, A. Comparison of two soft computing approaches for predicting CO_2 solubility in aqueous solution of piperazine. *Int. J. Greenhouse Gas Control* **2016**, *53*, 85−97.
(72) Ghiasi, M. M.; Arabloo, M.; Mohammadi, A. H.; Barghi, T. Application of ANFIS soft computing technique in modeling the CO_2 capture with MEA, DEA, and TEA aqueous solutions. *Int. J. Greenhouse Gas Control* **2016**, *49*, 47−54.
(73) Tatar, A.; Barati, A.; Yarahmadi, A.; Najafi, A.; Lee, M.; Bahadori, A. Prediction of carbon dioxide solubility in aqueous mixture of methyldiethanolamine and N -methylpyrrolidone using intelligent models. *Int. J. Greenhouse Gas Control* **2016**, *47*, 122−136.
(74) Wong, M. K.; Bustam, M. A.; Shariff, A. M. Chemical speciation of CO_2 absorption in aqueous monoethanolamine investigated by in situ Raman spectroscopy. *Int. J. Greenh. Gas Control* **2015**, *39*, 139−147.
(75) Song, H.-J.; Lee, S.; Maken, S.; Park, J.-J.; Park, J.-W. Solubilities of carbon dioxide in aqueous solutions of sodium glycinate. *Fluid Phase Equilib.* **2006**, *246*, 1−5.
(76) Mesbah, M.; Soroush, E.; Rostampour Kakroudi, M. Predicting physical properties (viscosity, density, and refractive index) of ternary systems containing 1-octyl-3-methyl-imidazolium bis-(trifluoromethylsulfonyl)imide, esters and alcohols at 298.15 K and atmospheric pressure, using rigorous classification techniques. *J. Mol. Liq.* **2017**, *225*, 778−787.
(77) Mesbah, M.; Soroush, E.; Rezakazemi, M. Development of a least squares support vector machine model for prediction of natural gas hydrate formation temperature. *Chin. J. Chem. Eng.* **2017**, *25*, 1238−1248.

https://doi.org/10.1021/acsomega.0c06158
ACS Omega 2021, 6, 12459−12469